# Wind Turbine Pitch Optimization

Benjamin Biegel Morten Juelsgaard Matt Kraning Stephen Boyd Jakob Stoustrup

***Abstract*— We consider a static wind model for a three-bladed, horizontal-axis, pitch-controlled wind turbine. When placed in a wind field, the turbine experiences several mechanical loads, which generate power but also create structural fatigue. We address the problem of finding blade pitch profiles for maximizing power production while simultaneously minimizing fatigue loads. In this paper, we show how this problem can be approximately solved using convex optimization. When there is full knowledge of the wind field, numerical simulations show that force and torque RMS variation can be reduced by over 96% compared to any constant pitch profile while sacrificing at most 7% of the maximum attainable output power. Using iterative learning, we show that very similar performance can be achieved by using only load measurements, with no knowledge of the wind field or wind turbine model.**

## I. Introduction

Wind turbines are expensive to build and maintain. The wind field from which they generate power is also the source of large fatigue loads on the turbine, which create structural wear and tear, increasing maintenance costs and decreasing the operational lifetime of the turbine. These costs are significant, and dramatically impact the profitability of the turbine. Many studies [1], [2], [3], [4], [5] have been performed which attempt to reduce fatigue loads while also generating sufficient power by dynamically controlling blade pitching. In this paper, we present a general blade pitching approach for fatigue load minimization based on convex optimization.

We focus on pitch controlled wind turbines, and investigate the use of pitching to obtain the maximum power output of a wind turbine. We then use this number to bound how much power must be sacrificed to achieve a given level of fatigue load reduction. We conclude by showing how iterative learning, using only load measurements, can achieve performance very close to that of a controller with perfect knowledge of the wind field and wind turbine model.

The first, second, and fifth authors are with the Department of Automation and Control, University of Aalborg, Aalborg, Denmark. Email: {biegel, juels, jakob}@es.aau.dk. The third and fourth authors are with the Information Systems Laboratory, Electrical Engineering Department, Stanford University, Stanford, CA 94305-9510, USA. Email: {mkraning, boyd}@stanford.edu.

## II. Wind Turbine Pitch Optimization

### A. Description

We consider a three-bladed, horizontal-axis, pitch-controlled wind turbine, as illustrated in figure 1. We assume that the wind turbine is affected by a wind field that is constant over time, but varying over the area swept by the blades. The blades of the rotor are numbered 1, 2, 3 and the angle $\theta \in [0, 2\pi/3]$ defines the position of the rotor.

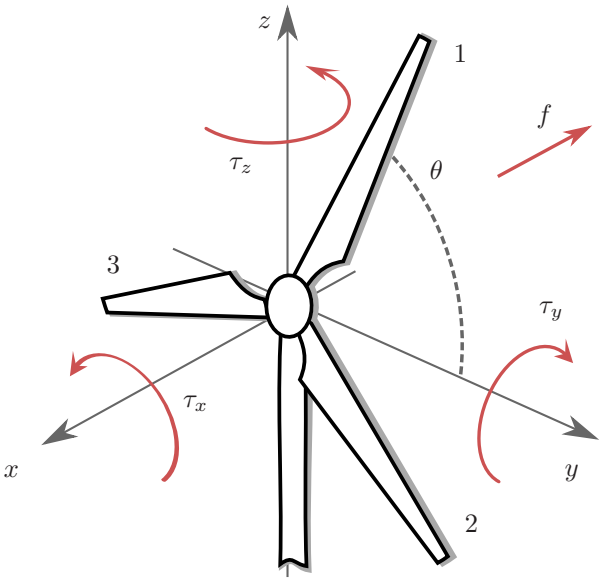


Fig. 1. Perspective view of a wind turbine.

The wind turbine is controlled via the pitch of the three blades. As the wind is assumed constant over time, the blade pitching is a periodic function of the angle $\theta$. We let

$$p(\theta) = \beta = (\beta_1, \beta_2, \beta_3) \in \mathbf{R}^3, \quad 0 \leq \theta \leq \frac{2\pi}{3}$$

denote the pitching angles of all three blades at angle $\theta$, where we suppress the explicit dependence of $\beta$ on the angle $\theta$. These pitch angles affect the generation of torques, $\tau = (\tau_x, \tau_y, \tau_z) \in \mathbf{R}^3$, around the three main axes and a net force, $f \in \mathbf{R}$, on the whole structure. The coordinate system is defined such that the $y$- and $z$-axes

span the rotor plane while the $x$-axis is perpendicular to the rotor plane, as in figure 1. The origin of our coordinate system is located at the intersection of the rotor plane with the axis of rotation.

During operation, $\tau$ and $f$ depend on the angle of the rotor, the pitch of the blades, the wind field present at the swept area, and the angular velocity of the rotor itself. We neglect the last dependency by assuming a constant rotor angular velocity and we let the wind field at the swept area be defined by the parameter vector $\eta$. Then $\tau$ and $f$ can be expressed by the functionals

$$\tau = \Psi(p(\theta), \theta, \eta), \quad f = \Upsilon(p(\theta), \theta, \eta).$$

In this work we use an overline to denote the mean value of a function of $\theta$ in the interval $0 \leq \theta \leq 2\pi/3$, *e.g.*

$$\overline{g} = \frac{3}{2\pi} \int_0^{2\pi/3} g(\theta) \, \mathrm{d}\theta,$$

and we overload this notation for vector valued functions componentwise.

The mean values $\overline{\tau}$ and $\overline{f}$ can be interpreted as DC-terms around which the torques and force vary. We define the AC-terms of the torques and force by

$$\delta\tau = \tau - \overline{\tau}, \quad \delta f = f - \overline{f},$$

respectively. At a given angle $\theta$, $\delta\tau$ and $\delta f$ depend not only on the pitch at this angle, but on the entire pitch profile $p(\theta)$ in the interval $0 \leq \theta \leq \frac{2\pi}{3}$, through the mean values $\overline{\tau}$ and $\overline{f}$. Using the root mean square (RMS) value of the AC-terms, we define the variation of the torques and force by $J = (J_x, J_y, J_z, J_f) \in \mathbf{R}^4_+$, where

$$J_x = \left(\overline{\delta\tau_x^2}\right)^{1/2}, \quad J_y = \left(\overline{\delta\tau_y^2}\right)^{1/2},$$
$$J_z = \left(\overline{\delta\tau_z^2}\right)^{1/2}, \quad J_f = \left(\overline{\delta f^2}\right)^{1/2}.$$

### B. Objectives

Wind turbine operation is a multiobjective optimization problem. First, we desire a large, even power output. As instantaneous power output is proportional to $\tau_x$, this corresponds to a large mean output torque, $\overline{\tau}_x$, with only small variations as measured by $J_x$. In addition, we want low mechanical fatigue on our structure in order to lengthen its operational lifetime and reduce maintenance costs. The torques $\tau_y$ and $\tau_z$ and force $f$ describe various mechanical loads experienced by the turbine structure. Their DC-terms are regarded as specifications which the wind turbine structure should be designed to handle and are therefore not treated in this work. The AC-terms of the mechanical loads cause structural fatigue. We therefore also want small RMS values of $\delta\tau_y$, $\delta\tau_z$, and $\delta f$, which are given by $J_y$, $J_z$, and $J_f$.

### C. Constraints

The pitch profiles are controlled by mechanical pitch actuators, which have limits in both range and pitch speed. We also assume that the wind turbine is not designed to operate in stall mode. These constraints can be expressed as

$$\beta_{\min} \leq p(\theta) \leq \beta_{\max},$$
$$\left|\tfrac{dp(\theta)}{dt}\right| \leq \beta_{\text{slew}},$$

where $\beta_{\min}$, $\beta_{\max}$ are, respectively, the minimum and maximum pitch angles that are operationally possible and at which the rotor will not stall, and $\beta_{\text{slew}}$ is the maximum pitch speed. We use $\mathcal{P}$ to denote the entire set of these constraints, which is a convex set.

## III. Model Description

In this section we consider the torque and force functionals, $\Psi(p(\theta), \theta, \eta)$ and $\Upsilon(p(\theta), \theta, \eta)$. We show how to find expressions for these functionals by forming a static model of the wind field and the wind turbine.

### A. Wind Model

Let the vector field $V_{\text{in}}(y, z) \in \mathbf{R}^3$ describe the incoming wind field at the area $\mathcal{A}$ swept by the turbine blades, where

$$\mathcal{A} = \{(x, y, z) \in \mathbf{R}^3 \mid x = 0, \ z^2 + y^2 \leq R^2\}$$

and $R$ is the length of each blade. We assume that the wind field has no $z$-component, and that the direction of the wind field is the same over the entire swept area. We further assume that the magnitude of the wind field can be described as a sum of wind phenomena contributions. The wind field is then given by

$$V_{\text{in}}(y, z) = (v_{\text{bl}} + v_{\text{vs}}(z) + v_{\text{hs}}(y) + v_{\text{ts}}(y, z))\,\vec{\Gamma}$$

where $\vec{\Gamma} = (\cos\gamma, \sin\gamma, 0)$, $\gamma$ is the direction of the wind, $v_{\text{bl}}$ is the baseline wind speed, $v_{\text{vs}}$ and $v_{\text{hs}}$ are respectively the vertical and horizontal shear, and $v_{\text{ts}}$ is the tower shadow. In the following, we describe the characteristics of the four wind phenomena.

*a) Baseline Wind Speed:* The baseline wind speed parameter $v_{\text{bl}} \in \mathbf{R}$ describes the wind speed at the origin of our coordinate system. All other wind terms are deviations from this value.

*b) Vertical Wind Shear:* The vertical wind shear parameter $\xi_{\text{vs}} \in \mathbf{R}$ describes the variation of wind speed as a function of altitude. This wind phenomena is known as wind shear [6]

$$v_{\text{vs}}(z) = v_{\text{bl}} \left[\xi_{vs}\left(\frac{z}{H}\right) + \frac{\xi_{vs}(\xi_{vs}-1)}{2}\left(\frac{z}{H}\right)^2 + \frac{\xi_{vs}(\xi_{vs}-1)(\xi_{vs}-2)}{2}\left(\frac{z}{H}\right)^3\right],$$

where $H$ is the height of the turbine hub above the ground.

*c) Horizontal Wind Shear:* The horizontal wind shear parameter $\xi_{hs} \in \mathbf{R}$ describes how the wind speed varies horizontally across the area swept by the blades. We assume a linear dependency between horizontal position and the horizontal wind shear, which is then given by

$$v_{\text{hs}}(y) = v_{\text{bl}}\xi_{hs}y.$$

*d) Tower Shadow:* The tower shadow parameter $t_s \in \{0, 1\}$ determines if the effect of the turbine tower on the wind field is included in the wind field model. The tower shadow is described by [1]

$$v_{ts}(y,z) = \begin{cases} -t_s \left(r_t \frac{d_t - y}{d_t + y}\right)^2 & z \leq 0, \\ 0 & \text{otherwise}, \end{cases}$$

where $r_t \in \mathbf{R}$ is the radius of the tower shaft, and $d_t \in \mathbf{R}$ is the distance of the rotor plane from the tower midline.

Using the static wind model above, we define the components of the wind parameter vector $\eta$ by

$$\eta = (\gamma, v_{\text{bl}}, \xi_{\text{vs}}, \xi_{\text{hs}}, t_s),$$

which fully specifies the wind field $V_{\text{in}}(y, z)$. Figure 2 illustrates an example wind field $V_{\text{in}}(y, z)$ over the swept area.

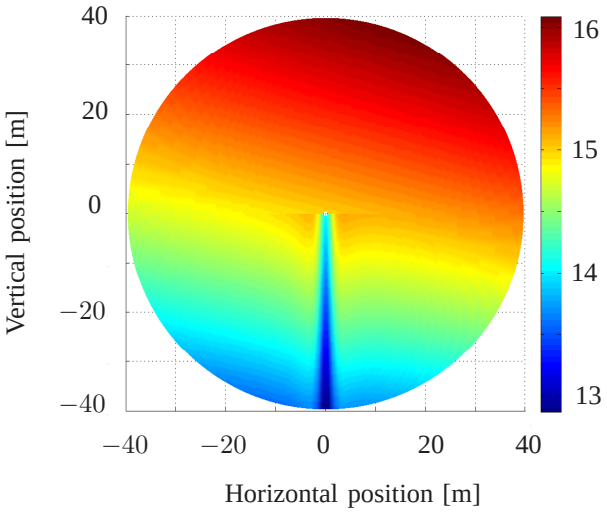


Fig. 2. Example of a wind field with wind parameter vector $\eta = [\gamma, v_{\text{bl}}, \xi_{\text{vs}}, \xi_{\text{hs}}, t_s] = [0, 15, 0.2, 5 \cdot 10^{-4}, 1]$ for a wind turbine with blade radius $R = 40$ m. The colors indicate the wind velocity in the range 13 to 16 m/s.

### *B. Turbine Model*

The wind velocity experienced by a wind turbine blade is known as the effective wind velocity and is defined as $V_{\text{eff}} = V_{\text{in}} + V_{\text{rot}} \in \mathbf{R}^3$, where $V_{\text{rot}} = (0, \omega_r r \sin\theta, \omega_r r \cos\theta) \in \mathbf{R}^3$ is the wind velocity due to the rotation of the blade itself and $\omega_r$ is the constant angular velocity of the rotor. When pitching a blade to an angle $\beta$, it is subjected to the forces [7]

$$dF_t = \frac{\rho}{2}\|V_{\text{eff}}\|_2^2 b \left(C_l(\alpha)\sin\psi - C_d(\alpha)\cos\psi\right) dr,$$
$$dF_a = \frac{\rho}{2}\|V_{\text{eff}}\|_2^2 b \left(C_l(\alpha)\cos\psi + C_d(\alpha)\sin\psi\right) dr,$$

where $dF_t,\ dF_a \in \mathbf{R}$ are the tangential and axial forces, respectively, acting on an infinitesimal blade element of length $dr$ and width $b$. The functions $C_l(\alpha)$ and $C_d(\alpha)$ are the lift and drag coefficients, respectively. They depend on the shape of the blade, and are functions of the wind angle of attack $\alpha$. The parameter $\rho$ is the density of air, while $\psi$ is the angle between $V_{\text{rot}}$ and $V_{\text{eff}}$. The blade also has a static pitch along its length, denoted $\beta_t$. Figure 3 illustrates these relations.

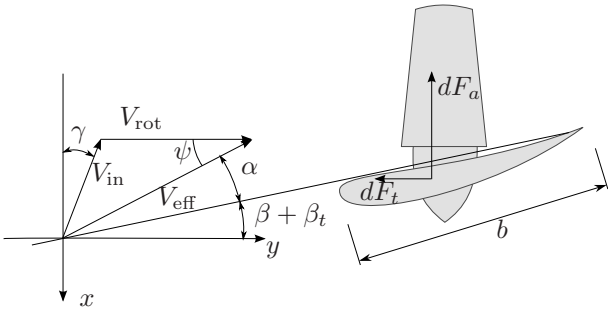


Fig. 3. Relations between the incoming wind and the the axial and tangential forces generated.

Once the axial and tangential forces acting on the blades are known, it is possible to form expressions for $\Psi(p(\theta), \theta, \eta)$ and $\Upsilon(p(\theta), \theta, \eta)$ for each blade [7]

$$\tau_x^i(\theta) = \int_{r=0}^{R} \Xi_i r \left(C_l(\alpha_i)\sin\psi_i - C_d(\alpha_i)\cos\psi_i\right) dr \quad (1)$$
$$\tau_y^i(\theta) = \int_{r=0}^{R} \Xi_i r\sin\theta \left(C_l(\alpha_i)\cos\psi_i + C_d(\alpha_i)\sin\psi_i\right) dr \quad (2)$$
$$\tau_z^i(\theta) = \int_{r=0}^{R} \Xi_i r\cos\theta \left(C_l(\alpha_i)\cos\psi_i + C_d(\alpha_i)\sin\psi_i\right) dr \quad (3)$$
$$f^i(\theta) = \int_{r=0}^{R} \Xi_i \left(C_l(\alpha_i)\sin\psi_i - C_d(\alpha_i)\cos\psi_i\right) dr, \quad (4)$$

where $\Xi_i = \frac{\rho}{2}\|V_{\text{eff},i}\|_2^2 b$, and $i \in \{1, 2, 3\}$ references quantities associated with blade $i$. The net force experienced by the turbine is given by $f(\theta) = \sum_{i=1}^{3} f^i(\theta)$, with similar expressions for the net torques.

## IV. Problem Formulation

### A. Power Maximization

We formulate the problem of maximizing mean output torque subject to physical blade pitching constraints as a convex optimization problem. Solutions to this problem will be used to evaluate power output reduction when reducing fatigue loads.

The power maximization problem can be formulated as

$$\begin{array}{ll} \text{maximize} & \overline{\tau}_x \\ \text{subject to} & p \in \mathcal{P} \end{array} \tag{5}$$

with variables $p(\theta) \in \mathbf{R}^3$ for $\theta \in [0, \frac{2\pi}{3}]$. In the model given by equations (1)-(4), $\overline{\tau}_x$ only depends on $p(\theta)$ through the lift and drag coefficients $C_l(\alpha)$ and $C_d(\alpha)$, an example of which are illustrated in figure 4 [8].

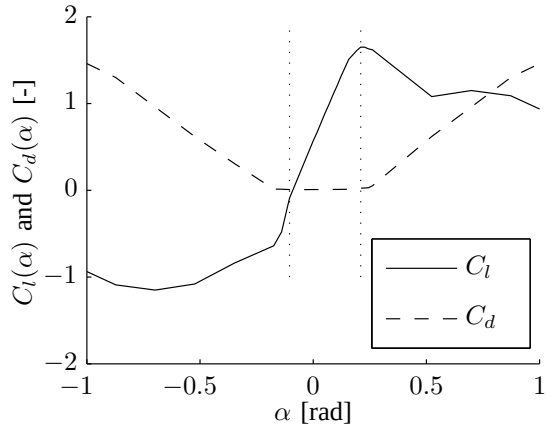


Fig. 4. Example lift and drag coefficient curves. The dotted lines indicate the interval in which the coefficients have been approximated.

The allowed range for $\alpha$ is limited, as operation in stall mode is prohibited. Using these limits, $C_l(\alpha)$ can be approximated by a concave function in $\alpha$, while $C_d(\alpha)$ can be approximated by convex function in $\alpha$. As $\tau_x$ is the sum of a positive weighting of the concave function $C_l(\alpha)$ and a negative weighting of the convex function $C_d(\alpha)$, $\tau_x$ and its mean value $\overline{\tau}_x$ are concave functions of $\alpha$, and thus also of $p(\theta)$. Since the constraint set $\mathcal{P}$ is convex, problem 5 is a convex optimization problem which can be solved globally and efficiently [9].

### B. Fatigue Load Minimization

In this section we address the problem of maximizing the mean output torque, while keeping it even and minimizing fatigue loads. This is a non-convex multiobjective optimization problem. We show how local solutions to this problem can be found by using sequential convex programming (SCP) [10].

Maximizing output power while minimizing fatigue loads and output power variation corresponds to maximizing $\overline{\tau}_x$ while simultaneously minimizing all components of $J$. We formulate this as the scalarized problem

$$\begin{array}{ll} \text{maximize} & \Phi(p) = \overline{\tau}_x - \lambda^T J \\ \text{subject to} & p \in \mathcal{P}, \end{array} \tag{6}$$

with variables $p(\theta) \in \mathbf{R}^3$ for $\theta \in [0, \frac{2\pi}{3}]$, and scalarization parameters $\lambda = (\lambda_x, \lambda_y, \lambda_z, \lambda_f) \in \mathbf{R}^4_+$. For simplicity, and to reflect the equal importance of both fatigue load minimization and even power output, we will use the scalarization parameters $\lambda = \mu\mathbf{1}$, $\mu \in \mathbf{R}_+$, for the remainder of this paper. By varying $\mu$, a trade-off curve between $\overline{\tau}_x$ and $\mathbf{1}^T J$ can be found. Unlike the power maximization problem, the additional objective term $\mathbf{1}^T J$ is non-convex and thus problem 6 is not a convex optimization problem. We therefore choose to solve it locally by using SCP.

The SCP method finds a local solution iteratively. At iteration $k$, a convex approximation of problem 6 is formed about a point $p^{(k)}$. This problem is formed by replacing the non-convex term $J$ by a convex approximation $\hat{J}^{(k)}$, which leads to the convex optimization problem

$$\begin{array}{ll} \text{maximize} & \hat{\Phi}(p) = \overline{\tau}_x - \mu\mathbf{1}^T \hat{J}^{(k)} \\ \text{subject to} & p \in \mathcal{P}, \\ & p \in \mathcal{T}^{(k)}, \end{array} \tag{7}$$

with variables $p(\theta) \in \mathbf{R}^3$ for $\theta \in [0, \frac{2\pi}{3}]$. The constraint set $\mathcal{T}^{(k)}$ is a (convex) trust region around the approximation point $p^{(k)}$ in which $\hat{J}^{(k)}$ is a sufficiently accurate approximation of $J$. The initial approximation point $p^{(0)}$ is typically chosen to be a point with reasonable performance, such as a well chosen constant pitch profile, and for subsequent values of $k$, $p^{(k)}$ is set equal to the solution of problem 7 at iteration $k-1$. By running a sufficient number of iterations, $p^{(k)}$ converges to a local optimum for problem 6 [11]. Although SCP is not guaranteed to find a globally optimal solution, it leverages the convex parts of the original non-convex problem, which often leads to a good solution.

## V. Numerical Examples

We present two numerical examples which solve discretized versions of the power maximization and fatigue load minimization problems. Starting from the model presented in equations (1)-(4), and using the wind field depicted in figure 2, we break each blade into $n$ smaller blade elements, and divide the swept area $0 \leq \theta \leq \frac{2\pi}{3}$ into $m$ discrete values. We approximate

$C_l(\alpha)$ and $C_d(\alpha)$ by piecewise linear concave and convex functions, respectively, with $d$ distinct segments. This allows all integrals to be replaced by finite sums and reduces the number of optimization variables to a finite and tractable number. For the specific examples we present, the parameter values $d = 40$, $m = 24$, and $n = 2$ were used, where the knot points of $C_l(\alpha)$ and $C_d(\alpha)$ were given by the model from [8]. Both example problems were solved using CVX [12].

We solved problem 5 to find the pitch profile $p^\star(\theta)$, which maximizes the mean output torque among all feasible pitch profiles. As problem 6 is only solved locally, the trade-off curve between $\overline{\tau}_x$ and $\mathbf{1}^T J$ depends on the initial pitch profile $p^{(0)}$ used in the SCP algorithm. For this reason, multiple initial pitch profiles were used as inputs for the SCP algorithm, and their corresponding trade-off curves are presented in figure 5. Good trade-off performance is obtained at the knee of figure 5, where very little power output is sacrificed to obtain significantly lower fatigue loads. We denote this pitch profile as $p^{\text{t.o.}}(\theta)$. Note that for every initial pitch profile, the SCP algorithm was able to find a final pitch profile that was very close to $p^{\text{t.o.}}(\theta)$. The pitch profiles $p^\star(\theta)$ and $p^{\text{t.o.}}(\theta)$ are shown in figure 6.

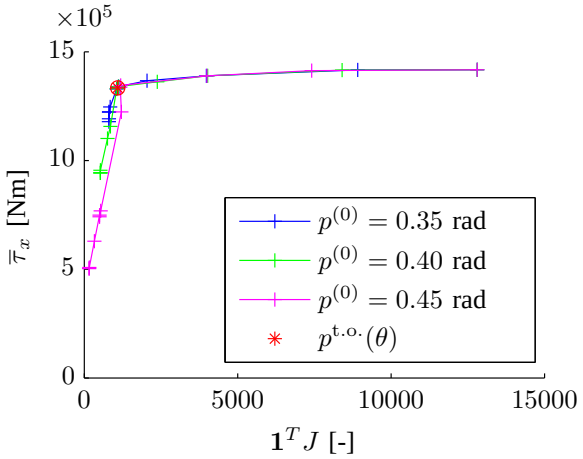


Fig. 5. Trade-off curves with different starting constant pitch profiles for the SCP algorithm. All initial starting points converged to $p^{\text{t.o.}}(\theta)$ for an appropriate choice of the tradeoff parameter $\mu$.

### A. Results

For the given wind field, we were able to find a constant pitch profile, $p^{c*}$, that was Pareto optimal (largest $\overline{\tau}_x$, smallest $\mathbf{1}^T J$) compared to all other constant pitch profiles. The torques and force generated by the pitch profiles $p^\star(\theta)$, $p^{\text{t.o.}}(\theta)$, and $p^{c*}$ are shown in figure 7.

Applying the pitch profile $p^\star(\theta)$ results in a mean output torque of $\overline{\tau}_x = 1.42 \cdot 10^6$ Nm, while the unit-weighted RMS variation for all AC-terms becomes $\mathbf{1}^T J = 1.28 \cdot 10^4$. By comparison, using the constant pitch profile $p^{c*}$ yields $\overline{\tau}_x = 1.41 \cdot 10^6$ Nm, and unit-weighted RMS variation of $\mathbf{1}^T J = 3.2 \cdot 10^4$. Thus, while the mean output torque is only increased slightly using the optimal pitch profile $p^\star(\theta)$ compared with $p^{c*}$, the undesirable AC-components of the torques and force are reduced by 60% using the torque-maximizing pitch profile $p^\star(\theta)$. This occurs even though RMS load minimization was not explicitly part of the objective function used to find $p^\star(\theta)$.

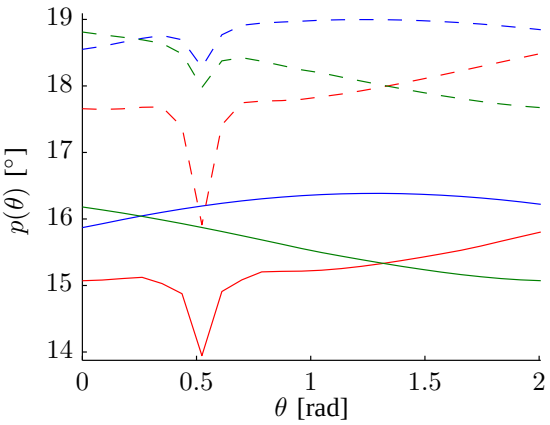


Fig. 6. The optimized pitch profiles $p^\star(\theta)$ (solid) and $p^{\text{t.o.}}(\theta)$ (dashed). The colors reference the same three blades in both profiles. The dip near 0.5 rad corresponds to the red blade passing through the area of the wind field that is significantly affected by the tower shadow.

Using the pitch profile $p^{\text{t.o.}}(\theta)$ results in an average output torque $\overline{\tau}_x = 1.33 \cdot 10^6$ Nm with a corresponding unit-weighted RMS variation $\mathbf{1}^T J = 1.10 \cdot 10^3$. Thus, the pitch profile $p^{\text{t.o.}}(\theta)$ reduces the unit-weighted RMS variation by more than 96% when compared to any constant pitch profile, while also having a mean output torque that is only 7% less than what can be generated by any pitch profile.

Looking at the pitch profiles in figure 6, and the corresponding torques and force experienced by the wind turbine in figure 7, we see that most of the RMS variation occurs when a blade passes through the area of the wind field significantly affected by the tower shadow. By having all three blades coherently adjust their pitches when one blade passes through the tower shadow, $p^{\text{t.o.}}(\theta)$ is able to achieve effectively zero variation in all torques.

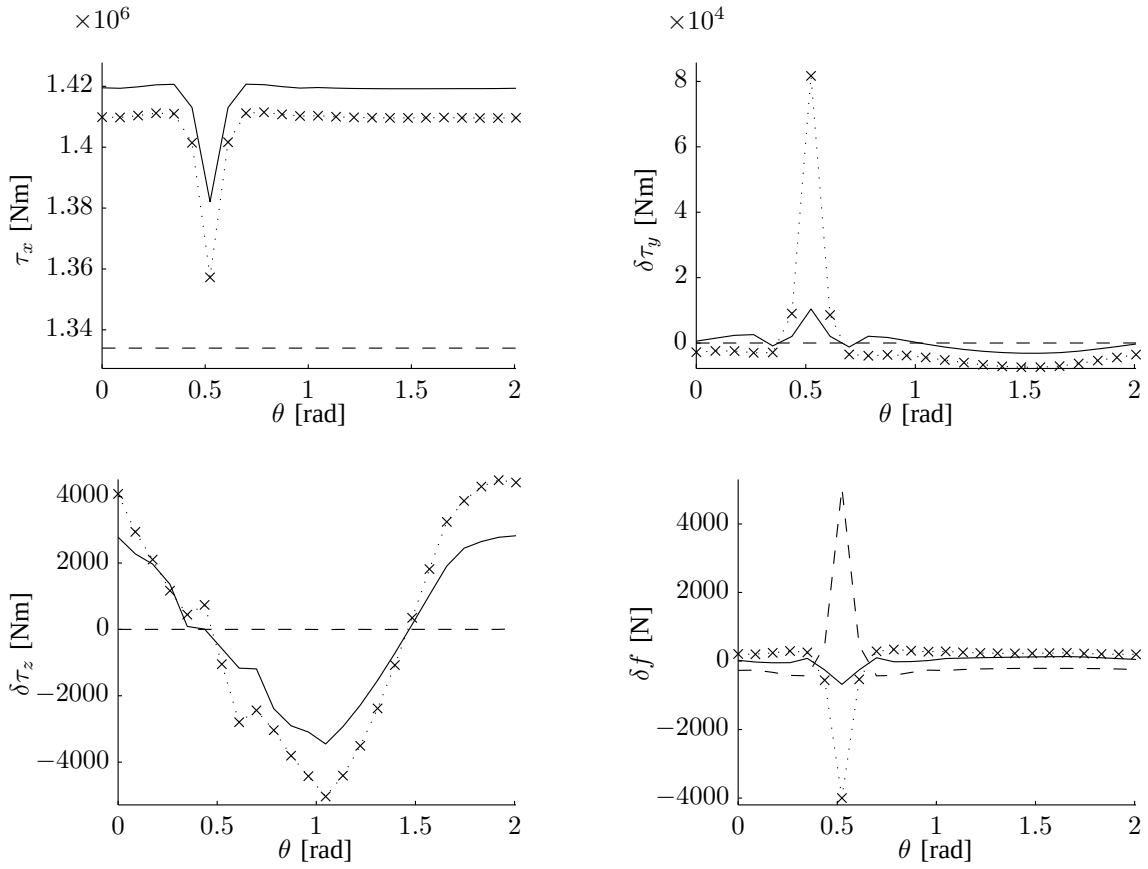


Fig. 7. Torques and force resulting from the pitch profiles $p^\star(\theta)$ (solid), $p^{\text{t.o.}}(\theta)$ (dashed), and $p^{\text{c}*}$ (dotted X's).

## VI. Iterative Learning Control

In the previous sections we assumed perfect knowledge of the wind field and turbine model when calculating pitch profiles. In this section we show that pitch profiles can be computed solely from load measurements, with no prior knowledge of the wind field or underlying turbine model. We do this through a simple implementation of iterative learning control (ILC). For a more thorough examination of ILC and extremum-seeking control, refer to [13], [14], and [15].

### A. Model

We consider the wind turbine positioned at a fixed angle $\theta$. There exists an unknown mapping $\phi$ from the the pitch $\beta \in \mathbf{R}^3$ to the AC-terms $e = (\delta\tau, \delta f) \in \mathbf{R}^4$, such that

$$e = \phi(\beta).$$

At each $\theta$, the term $e$ can be seen as an error. We want to minimize this error $e$ for all $\theta$, thereby minimizing the AC-load $\mathbf{1}^T J$. We do this iteratively by using ILC. This is a two step process: we first estimate the function $\phi$, and then find the pitch $\beta$ that minimizes the estimated $\phi$.

### B. Estimation

The mapping $\phi$ is unknown, but we approximate it by an affine expression at an operating point $\beta^o$ such that

$$\phi(\beta) \approx \phi(\beta^o) + D\phi(\beta^o)(\beta - \beta^o),$$

where $D\phi(\beta^o) \in \mathbf{R}^{4\times 3}$ is the Jacobian of $\phi$ at $\beta^o$. By taking a sequence of measurements of the error $e = \phi(\beta)$ over a range of $\beta$, we can estimate this affine approximation of $\phi(\beta)$ via least squares.

We assume that a desired power set-point is provided for the mean output torque $\overline{\tau}_x$, which is predetermined based on the wind conditions. Along with this set-point, the mean values $\overline{\tau}_y, \overline{\tau}_z$, and $\overline{f}$ are required in order to determine the error, as $e = (\tau - \overline{\tau}, f - \overline{f})$. These quantities are updated dynamically during turbine operation after each full rotation. This allows the mean

values to change if, for example, the wind field changes. The mean value updates are given by

$$\begin{aligned}\overline{\tau}_y &:= (1-q)\overline{\tau}_y + q\overline{\tau}_y^{\text{meas}},\\ \overline{\tau}_z &:= (1-q)\overline{\tau}_z + q\overline{\tau}_z^{\text{meas}},\\ \overline{f} &:= (1-q)\overline{f} + q\overline{f}^{\text{meas}},\end{aligned}$$

where $\overline{\tau}_y^{\text{meas}}, \overline{\tau}_z^{\text{meas}}, \overline{f}^{\text{meas}} \in \mathbf{R}$ are the mean torque and force values measured over the last full rotation, and $q \in [0,1]$ is a smoothing parameter.

### C. Optimization

We wish to find the pitch $\beta$ that minimizes the approximation of $\phi$. In order to maintain the accuracy of the approximation, we also want $\beta$ to be located close to the operating point $\beta^o$. We can formulate this problem as

$$\text{minimize} \quad \|\phi(\beta^o) + D\phi(\beta^o)(\beta - \beta^o)\|_2^2 + \nu\|\beta - \beta^o\|_2^2,$$

with variable $\beta \in \mathbf{R}^3$, where $\nu \in \mathbf{R}$ is a trade-off parameter, and $\phi(\beta^o) \in \mathbf{R}^4, D\phi(\beta^o) \in \mathbf{R}^{4\times 3}, \beta^o \in \mathbf{R}^3$ are the problem data. The solution to this problem, $\beta^\star$, can be found analytically

$$\beta^\star = \beta^o - (D\phi(\beta^o)^T D\phi(\beta^o) + \nu I)^{-1} D\phi(\beta^o)^T \phi(\beta^o).$$

This forms the basis for our ILC algorithm. We let

$$H(\beta^o) = (D\phi(\beta^o)^T D\phi(\beta^o) + \nu I)^{-1} D\phi(\beta^o)^T \phi(\beta^o)$$

and introduce a learning rate $\kappa \in [0,1]$ such that

$$\beta = \beta^o - \kappa H(\beta^o)\phi(\beta^o). \tag{8}$$

This expression exists for every $\theta \in [0, \frac{2\pi}{3}]$.

### D. Algorithm

We implemented ILC on the same discretized turbine model from the previous section, in which each discretized angular subinterval individually ran the control method described in equation (8). Every time a blade passed through an interval corresponded to an iteration in the ILC algorithm running in that interval. At iteration $k$ we applied the pitch $\beta^{(k)}$ and measured the error $e^{(k)}$. We then set $\beta^{(k)}$ as the operating point and used equation (8) to find $\beta^{(k+1)}$.

For this example, we used the simplification $H = H(\beta^{(k)}) = H(\beta^o)$, *i.e.* we estimated $H$ offline for some pitch $\beta^o$, and used this regardless of the current operating point $\beta^{(k)}$. The ILC algorithm then became

$$\beta^{(k+1)} := \beta^{(k)} - \kappa H e^{(k)}.$$

### E. Results

We applied ILC under the same initial wind conditions in our previous numerical examples. Figure 8 shows how the AC-load and set-point tracking evolved over the course of 50 rotations. After 20 rotations, the AC-load quickly decreased from $2.94 \cdot 10^4$ Nm to $2.80 \cdot 10^3$ Nm while the mean torque $\overline{\tau}_x$ stabilized to within $1\%$ of its set-point value, $1.33 \cdot 10^6$ Nm. This corresponds to a $91\%$ reduction in RMS variation when compared to $p^{c*}$, while having the same mean torque as $p^{\text{t.o.}}(\theta)$.

After 22 rotations the baseline wind speed $v_{\text{bl}}$ was increased. The AC-load increased briefly, after which it quickly reduced due to adaption. Even though the same matrix $H$ was used through all iterations, good performance was obtained, even for different wind fields.

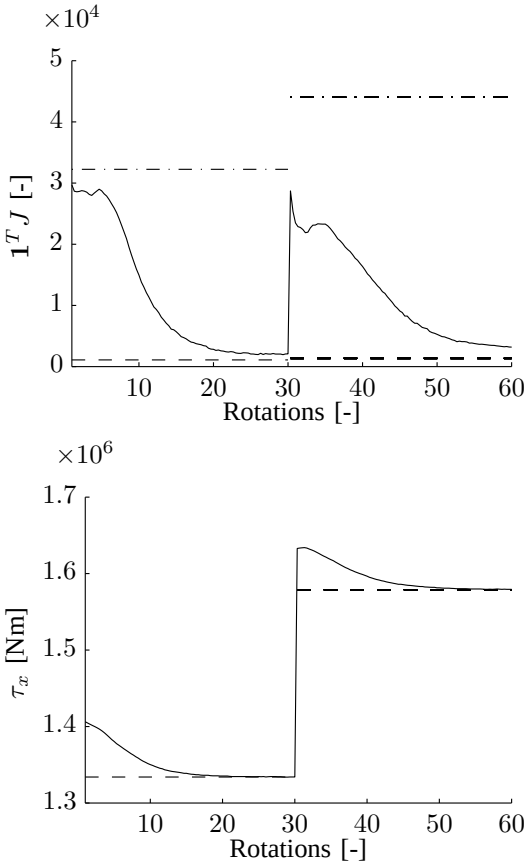


Fig. 8. (Top) The AC-load $\mathbf{1}^T J$ evaluated after each full rotation (solid) compared to the response of using constant pitch profile (dotted dash) and using the optimized pitch profile $p^{\text{t.o.}}(\theta)$ (dashed). (Bottom) The output torque $\tau_x$ (solid), along with the set-points (dashed).

## VII. Conclusion

We have presented methods for choosing pitch profiles that maximize power production and minimize

RMS load variations for a static wind turbine model. By choosing an optimized pitch profile, force and torque RMS variation can be reduced by over 96% percent compared to any constant pitch profile, while only forfeiting 7% of the maximum power output. Moreover, we have shown that simple iterative learning, using only load measurements, can achieve $91\%$ RMS variation reductions with the same mean output torque as that of a profile optimized with full knowledge of the wind field and wind turbine model. Lastly, the learning controller quickly adapts to wind field changes, showing the robustness of our method to dynamic wind conditions.

## VIII. Acknowledgements

This material is based on work supported by JPL contract 1400723, by AFOSR grant FA9550-09-0130, and by AFOSR grant FA9550-06-1-0312.

## References

[1] T. Burton, D. Sharpe, N. Jenkins, and E. Bossanyi, *Wind Energy Handbook*. Wiley, 2001.

[2] H. Wang, W. Wang, and L. Bin, "Application of individual pitch controller for flicker reduction on variable speed wind turbines," *Power and Energy Engineering Conference (APPEEC), 2010 Asia-Pacific*, March 2010.

[3] S. Nourdine, H. Camblong, I. Vechiu, and G. Tapia, "Comparison of wind turbine LQG controllers using individual pitch control to alleviate fatigue loads," *18th Mediterranean Conference on Control & Automation*, June 2010.

[4] Y. Xingjia, W. Xiaodong, X. Zuoxia, L. Yingming, and L. Jun, "Individual pitch control for variable speed turbine blade load mitigation," *Sustainable Energy Technologies, ICSET 2008. IEEE International Conference.*, November 2008.

[5] M. Jelavić, V. Petrović, and N. Perić, "Individual pitch control of wind turbine based on loads estimation," *Industrial Electronics, 2008. IECON. 34th Annual Conference of IEEE*, November 2008.

[6] D. S. L. Dolan and D. P. W. Lehn, "Simulation model of wind turbine 3p torque oscillations due to wind shear and tower shadow," *IEEE Transactions on energy conversion*, vol. 21, no. 3, p. 8, September 2006.

[7] M. Stiebler, *Wind Energy Systems for Electric Power Generation*. Springer, 2008.

[8] J. Jonkman, "Fast - an aeroelastic design code for horizontal axis wind turbines," Webpage, 2010, http://wind.nrel.gov/designcodes/simulators/fast/.

[9] S. Boyd and L. Vandenberghe, *Convex Optimization*. Cambridge University Press, 2004.

[10] S. Boyd, "Sequential convex programming," http://www.stanford.edu/class/ee364b/lectures/seq_slides.pdf, 2008.

[11] R. H. Byrd, J. C. Gilbert, and J. Nocedal, "A trust region method based on interior point techniques for nonlinear programming," *Mathematical Programming Series A*, vol. 89, no. 1, pp. 149–185, 2000.

[12] M. Grant and S. Boyd, "CVX: Matlab software for disciplined convex programming, version 1.21," http://cvxr.com/cvx, Feb. 2011.

[13] H. Ahn, Y. Chen, and K. L. Moore, "Iterative learning control: Brief survey and categorization," *IEEE Transactions on Systems, Man, and Cybernetics, Part C: Applications and Reviews*, vol. 37, no. 6, pp. 1099–1121, November 2007.

[14] D. A. Bristow, M. Tharayil, and A. G. Alleyne, "A survey of iterative learning control a learning-based method for high-performance tracking control," *IEEE control systems magazine*, vol. 26, no. 3, pp. 96–114, June 2006.

[15] K. B. Ariyur and M. Krstić, *Real-Time Optimization by Extremum-Seeking Control*. Wiley, 2003.